polymer papers

# Formation and break-up of a bead-and-string structure during injection moulding of a polycarbonate/acrylonitrile–butadiene–styrene blend

**M.-P. Lee, A. Hiltner* and E. Baer**
*Department of Macromolecular Science, and Center for Applied Polymer Research, Case Western Reserve University, Cleveland, OH 44106, USA*
*(Received 26 December 1990; accepted 27 January 1991)*

The morphology gradient through the thickness of an injection-moulded blend of 10% by weight acrylonitrile–butadiene–styrene (ABS) and 90% by weight polycarbonate (PC) has been characterized. Brittle fracture surfaces were etched and examined both parallel and perpendicular to the injection direction in the scanning electron microscope. In the centre of the plaque, the morphology was isotropic with the ABS phase dispersed in the PC matrix as large composite rubber particles about 1 $\mu$m in diameter and smaller particles of free styrene–acrylonitrile (SAN) about 0.3 $\mu$m in diameter. About half the distance from the centre to the edge, the morphology of the free SAN phase changed from predominantly spherical to predominantly string-like. The SAN strings connected the rubber particles to form an oriented ABS bead-and-string structure that was essentially continuous in the injection direction. It was thought that the free SAN was highly extended under elongational or shear flow while remaining attached to the rubber particles because of miscibility with grafted SAN. The bead-and-string structure was retained near the edge where the melt solidified most rapidly. In the centre of the plaque, the low shear rate during mould filling and longer cooling time after mould filling favoured relaxation of the bead-and-string structure. The morphology gradient through the thickness was created by the competition between the relaxation rate and the cooling rate after mould filling. In this case, relaxation was thought to occur by interfacial-tension-driven break-up and end-pinching mechanisms to produce the dispersion of rubber and free SAN particles. Evidence to support the break-up mechanism was obtained when annealing above the glass transition temperature of PC for a matter of seconds, the timescale of mould cooling, caused the bead-and-string structure to convert to a dispersion of composite rubber particles and SAN particles.

**(Keywords: acrylonitrile–butadiene–styrene; polycarbonate; blend morphology; injection moulding; Rayleigh instability)**

## INTRODUCTION

Injection moulding is one of the most important plastics fabrication operations, and is frequently employed for melt-forming blends of immiscible polymers. Although it is well known that the improved physical and mechanical properties of polymer blends are highly dependent on the phase morphology, the non-steady-state conditions during injection moulding make it particularly difficult to predict and control the solid-state morphology achieved in injection-moulded parts. Material properties of the components, such as interfacial tension and rheological characteristics, have a major effect on size and shape of domains that are formed by the complex shear and elongational flow fields of the mould filling process. After cessation of flow, the domain morphologies created by the flow patterns during mould filling relax to a greater or lesser extent depending upon the rate of cooling. As a result, skin–core structures that have a gradient in phase morphology through the thickness are characteristic of injection-moulded parts.

Elongated domains of the dispersed component are frequently observed in the skin at the mould-contacting surface where the melt experiences elongational flow at the front of the fountain flow pattern[1] and where rapid freezing favours retention of the melt morphology in the solid state. For example, dispersed particles of ethylene–propylene–diene terpolymer (EPDM) in polypropylene were observed to be highly elongated in the skin layer[2], as were styrene–acrylonitrile (SAN) domains in blends with polycarbonate (PC)[3,4]. When other variables are held constant, the viscosity ratio of the two components is the decisive factor controlling the extent to which the dispersed phase is elongated in the flowing melt[5]. The elongated domain morphology is sustained by the flow field, but after cessation of flow may relax to a spherical shape. Or, if the aspect ratio is sufficiently large, it has been suggested that the domains may break up by an interfacial instability mechanism[6–8], which has been described analytically for Newtonian liquids[9–12].

Blends with acrylonitrile–butadiene–styrene (ABS) as one of the components have an additional complication in that the ABS is itself a heterogeneous material and consists of a free SAN component together with composite rubber particles with a grafted SAN shell and SAN sub-inclusions. Because of the recent interest in blends of PC with ABS[13–15], a study has been undertaken to characterize the morphology gradient through the thickness of an injection-moulded blend of PC with

* To whom correspondence should be addressed

0032-3861/92/040675-10

10 wt% ABS, and to find an explanation for the phase morphology that considers the processing parameters.

## EXPERIMENTAL

A blend with 10% by weight ABS and 90% by weight PC was provided by The Dow Chemical Company in the form of injection-moulded 5 inch (12.7 cm) × 3 inch (7.6 cm) × 1/8 inch (0.3 cm) plaques. A tab was located at one end in the centre of the width and a conventional rectangular edge gate fed this tab. The plaques were moulded with an Arburg model 300-210-700 injection-moulding machine with a screw rotational speed of 300 rpm. The injection pressure was 55 bar, the melt (barrel) temperature about 270°C and the mould temperature was 79.5°C. The total cycle time of 27.5 s consisted of a delayed injection time of 0.5 s, an injection time of 4 s, a packing time of 4 s, a cooling time of 18.0s and a 1.0 s pause after mould opening.

The polymers were a commercial grade of polycarbonate (Calibre® from The Dow Chemical Company) with melt flow index of 10 g $min^{-1}$ (ASTM 1238 condition O) and a commercial ABS resin from The Dow Chemical Company reported by the manufacturer to be about 20% by weight acrylonitrile and 20% by weight butadiene rubber. Following a published method[16], the ABS resin was dispersed in acetone to dissolve free SAN and the milky solution repeatedly centrifuged until a clear supernatant liquid was obtained. The insoluble composite rubber particles were separated from the acetone-soluble fraction by decanting the clear liquid, and were then dried and weighed.

The compositions of the ABS and the soluble SAN component were determined by infra-red analysis. Films were cast from tetrahydrofuran (THF) solution and the spectra obtained on a DigiLab Biorad FTS-60. The weight ratio of butadiene to styrene in ABS was determined from the absorbance ratio of bands at 968 $cm^{-1}$ and 3077 $cm^{-1}$ (ref. 17). When the styrene is above 75%, this ratio can also be obtained from the absorbance ratio of bands at 968 $cm^{-1}$ and 1030 $cm^{-1}$ (ref. 18). Both determinations were made for internal consistency. The relative weight fraction of acrylonitrile to styrene either in free SAN or in ABS was obtained from the absorbance ratio of the 2220 $cm^{-1}$ and 755 $cm^{-1}$ bands[19]. Calibration curves were constructed from commercial resins of known composition. Analysis of the ABS resin showed it to be about 15% rubber by weight and 20% by weight acrylonitrile. Of the 85% of the ABS that was SAN, 79% was present as free SAN and 21% was associated with the rubber either as grafted SAN or as occluded SAN particles. The free SAN was estimated to be 25% acrylonitrile.

The number- and weight-average molecular weights of PC and the soluble SAN fraction of the ABS were measured with a Varian DS 651 g.p.c. relative to polystyrene standards at 25°C using THF as the solvent. The weight-average molecular weight of the SAN relative to polystyrene was about $1.4 \times 10^5$ with a polydispersity of 2.3, and that of PC was $5.6 \times 10^4$ with a polydispersity of 1.9.

Tensile specimens were cut to the ASTM 1708 geometry either parallel or perpendicular to the injection direction. A single edge notch (SEN) was machined at the midpoint of the gauge length: the notch was 0.037 inch (0.094 cm) in depth with a 0.010 inch (0.025 cm) notch radius and 45° flank angle. The specimens were cut and notched in such a way that the location of fracture was through the thickness at the centre of the plaque. The notched tensile specimens were fractured in the Instron at −70°C with a crosshead speed of 229 mm $min^{-1}$. The brittle cryogenic fracture surfaces were subsequently selectively etched by immersion in 30% by weight aqueous potassium hydroxide for approximately 5 h, dried, coated with gold and examined in the JEM 35CF scanning electron microscope (SEM). Alternatively, some of the etched specimens were stained with a 1% by weight aqueous solution of osmium tetroxide at room temperature for two weeks, then coated with gold and examined in a JEOL 840A scanning electron microscope in the backscatter mode. One of the brittle fracture surfaces that had been etched with aqueous KOH was subsequently etched with acetone to remove free SAN, then washed in water, dried, coated with gold and viewed in the SEM.

In some cases, the plaque was sectioned with a diamond wafering blade on the Isomet from the Buehler Company, then etched with aqueous KOH, washed with water, dried and coated with gold for viewing in the SEM. This procedure was used to examine the phase morphology in the tab of the injection-moulded plaque. The plane parallel to the mould-contacting surface was sectioned with the RMC MT-6000-XT cryogenic ultramicrotome.

Annealing experiments were carried out on rectangular specimen blocks cut from the centre of the plaque with the wafering blade. The specimen block was positioned in a large d.s.c. pan so that the surface cut through the thickness parallel to the injection direction contacted the bottom of the pan. In this way, the surface of interest was as close as possible to the d.s.c. heating element and differences between the programmed temperature and the actual temperature experienced by the specimen were minimized as much as possible. Annealing was carried out in the Perkin–Elmer DSC-7; the specimen was heated to the annealing temperature of 185, 200 or 270°C at a heating rate of 200°C $min^{-1}$, held at that temperature for 6 or 12 s, then cooled to ambient temperature at a rate of 200°C $min^{-1}$. The surface of the specimen block that had contacted the bottom of the pan was etched with aqueous KOH, washed, dried and coated with gold for viewing in the SEM.

## RESULTS AND DISCUSSION

### *Morphology*

Brittle fracture surfaces both parallel and perpendicular to the injection direction were etched to remove the PC phase and viewed in the SEM to characterize the morphology gradient through the thickness of the plaque. Although the morphology probably varied to some extent along the length and width of the plaque, this was not examined and the midpoint of the plaque was chosen as a representative location. At the centre of the plaque, the morphology appeared the same in both parallel and perpendicular directions (*Figures 1a* and *1b*). When the PC was etched away, the ABS phase was revealed to be discontinuous and to consist of two populations of spherical particles: a relatively small number of larger spheres approximately 1 $\mu$m in diameter together with numerous small particles with a diameter of about 0.3 $\mu$m.

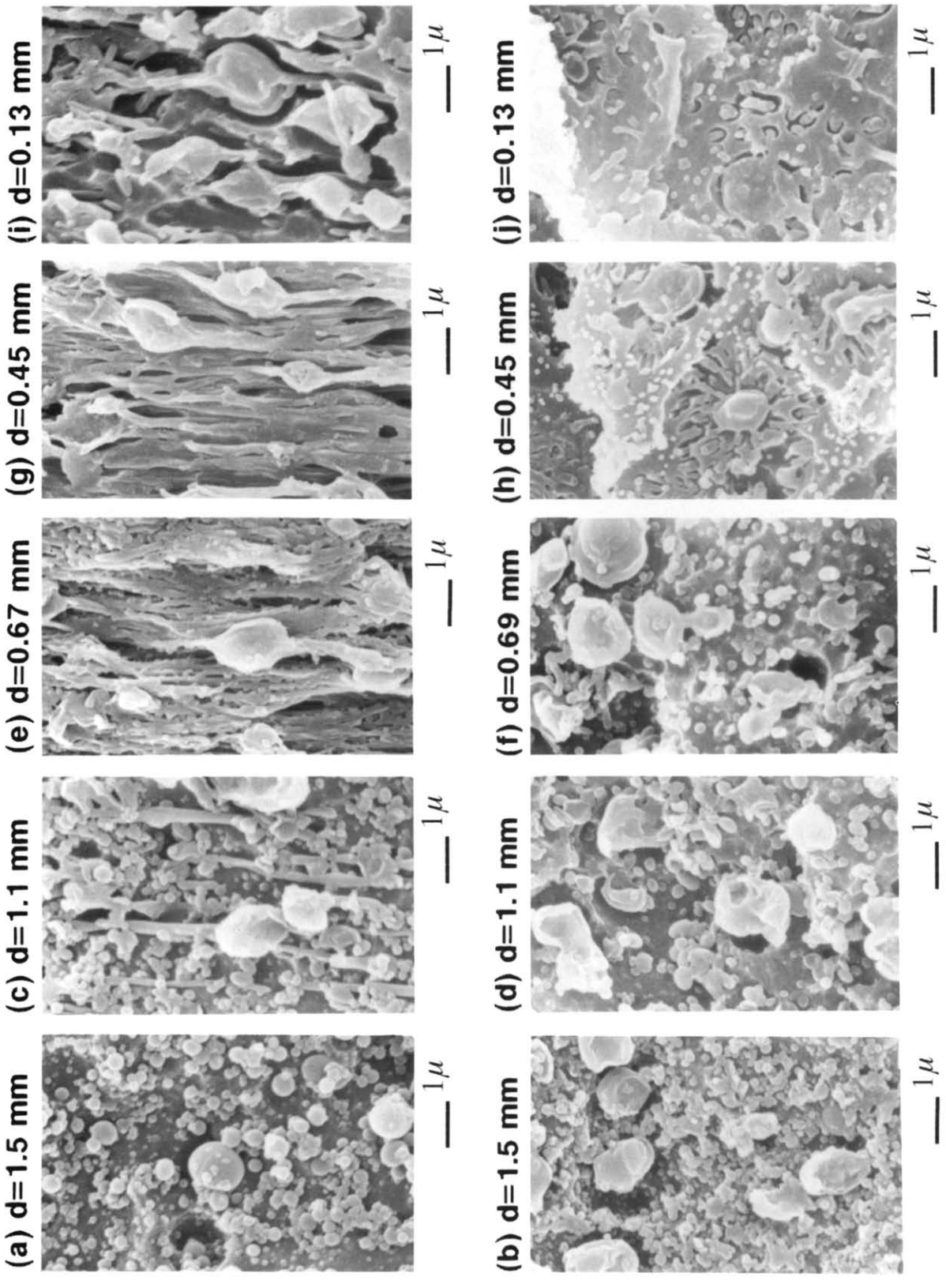


**Figure 1** Scanning electron micrographs of the injection-moulded PC/ABS 90/10 blend at various positions through the thickness; (a), (c), (e), (g) and (i) parallel to the injection direction; and (b), (d), (f), (h) and (j) perpendicular to the injection direction. The distance *d* from the edge of the 3 mm plaque is indicated with each micrograph

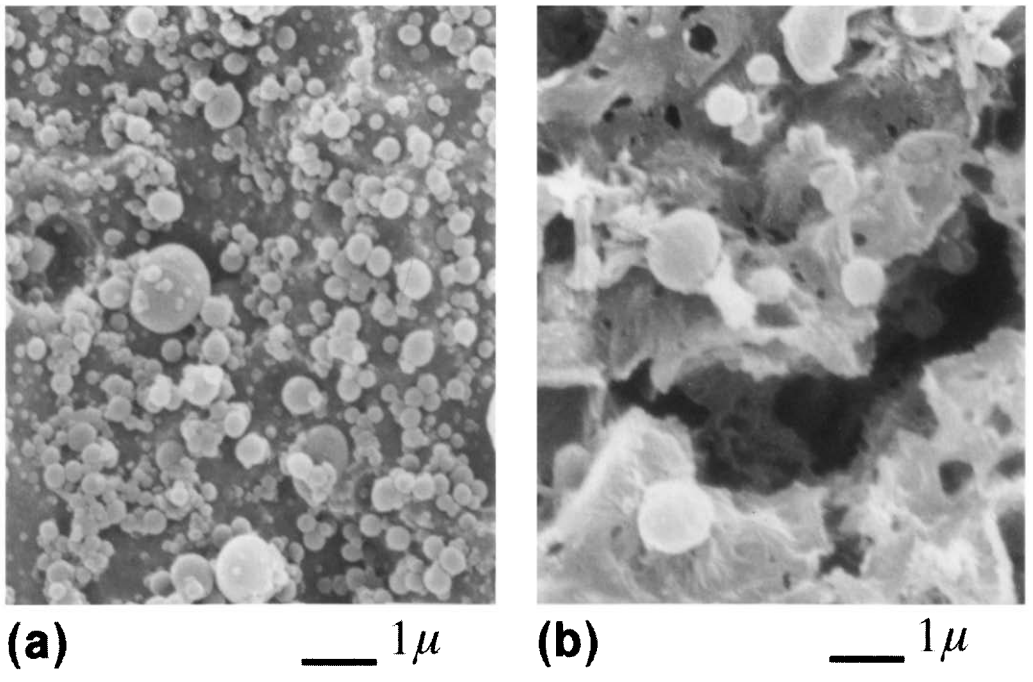


**Figure 2** Views parallel to the injection direction near the centre of the plaque: (a) etched with KOH to remove PC; and (b) etched with KOH and subsequently etched with acetone to remove free SAN

In addition to the large and small particles, some string-like domains elongated in the injection direction and about 0.2 $\mu$m in diameter were visible in the parallel view at a position 1.05 mm from the edge of the 3 mm thick plaque (*Figure 1c*). The string-like domains were not readily apparent in the perpendicular view from a similar location (*Figure 1d*). In this view, the ABS domains appeared very much as they did in the centre of the plaque (cf. *Figure 1b*), although there was occasionally the suggestion that a small particle was actually the end of an elongated domain.

Midway between the edge and centre of the plaque, at 0.84 mm (not shown) and 0.67 mm from the edge, the elongated domains were much more numerous in the parallel views and sometimes were attached to the large 1 $\mu$m particles (*Figure 1e*). Fewer of the smaller 0.3 $\mu$m particles were observed in this region, and they frequently appeared to be part of string-like domains. The corresponding perpendicular view (*Figure 1f*) differed only subtly from those closer to the centre of the plaque. Close examination showed that many of the small particles, which had the same diameter as the strings in the parallel view, were the protruding ends of elongated domains.

The small spherical particles were not observed in parallel views closer to the edge; at 0.53 mm (not shown) and 0.45 mm from the edge of the plaque the morphology of the ABS phase consisted of densely packed string-like domains connecting the large spherical particles (*Figure 1g*). This 'bead-and-string' morphology created ABS domains that were essentially continuous in the injection direction. Circular cross-sections and protruding ends of strings were seen in the corresponding perpendicular view (*Figure 1h*). This view also showed star-like arrays with numerous strings emanating from the large 1 $\mu$m particle; these appeared to produce interconnections among bead-and-string structures.

The bead-and-string structure was also observed near the edge but with subtle differences. Parallel views 0.20 mm (not shown) and 0.13 mm from the edge were indistinguishable and showed that close to the edge the string-like domains were more discrete and less interconnected (*Figure 1i*). This was confirmed in the perpendicular view (*Figure 1j*), where on the average there were fewer strings attached to the large particles.

The ABS component was itself heterogeneous and consisted of free SAN and composite rubber particles with a grafted SAN shell and SAN sub-inclusions. The SEM backscatter images showed the large 1 $\mu$m spheres to be selectively stained by $OsO_4$, which identified them as the rubber particles. In order to differentiate further the free SAN from the composite rubber particles, brittle fracture surfaces that had been etched with aqueous KOH to remove PC were subsequently etched with acetone to remove the free SAN. Comparison of a parallel view from the centre before the surface was etched with acetone (*Figure 2a*) with a view of the same region after etching with acetone (*Figure 2b*) showed that acetone removed the numerous small particles but not the large ones. A similar comparison of regions with the bead-and-string structure near the edge of the plaque showed that acetone removed the strings. This identified the small particles in the centre part of the plaque and the string-like domains in the edge region as the free SAN component of the ABS phase.

The predominant feature of the morphology gradient through the thickness of the plaque was the change in the free SAN component from 0.3 $\mu$m spheres in the centre to strings connecting rubber particles in the bead-and-string structure nearer the edge. To illustrate the change in morphology through the thickness, the number density of SAN spheres was measured from the parallel micrographs at various positions (*Figure 3*). While the absolute numbers are not significant, they do show that, while there were essentially no spherical particles near the edge, at about 0.5 mm in from the edge

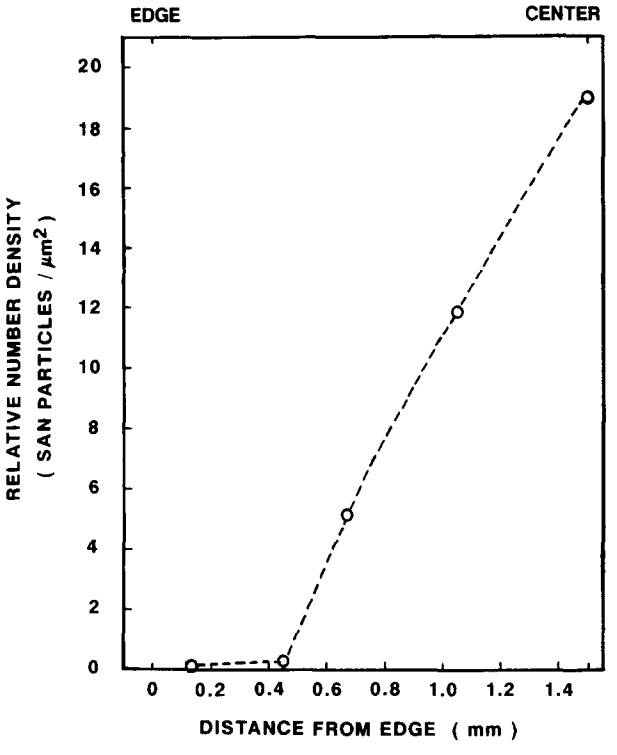


**Figure 3** The relative number density of spherical SAN particles on micrographs of a parallel fracture surface at various positions through the thickness of the plaque

the relative number density of free SAN particles began to increase rapidly and continued to increase to the centre.

A model of the gradient morphology through the thickness of the plaque was developed (*Figure 4*). In the centre, the morphology was isotropic in the parallel and perpendicular directions with the ABS phase dispersed in the PC matrix as large composite rubber particles and smaller spherical SAN particles. Away from the centre, a few string-like SAN domains elongated in the injection direction appeared, and about half the distance from the centre to the edge, the morphology of the free SAN phase changed from predominantly spherical to predominantly string-like. The SAN strings connected the rubber particles to form an ABS bead-and-string morphology that was essentially continuous in the injection direction. The bead-and-string structure was highly interconnected, although in a 0.2 mm thick region at the edge of the plaque a subtle change occurred and the strings of the bead-and-string structure were more discrete with fewer interconnections.

*Formation of bead-and-string structure*

The shear-rate-dependent viscosity was estimated from methods described in the literature. The influence of acrylonitrile content on the flow curve of SAN is reportedly very slight[20]; the shift factor for molecular weight from Casale *et al.*[20] was used to obtain the viscosity at the reference temperature of 210°C, and with the temperature shift factor from Mendelson[21], which is reportedly independent of both molecular weight and acrylonitrile content, the rheological behaviour at the injection temperature was determined. The flow curve of the PC component was estimated from the melt flow index using the parameters reported by Shenoy and Saini[22,23]. The estimated viscosity ratio of free SAN to PC at the injection temperature, 270°C, varied from 0.4 to 0.3 over the range of shear rates from 3 to $10^3$ $s^{-1}$.

In a blend that was 90% PC and only 10% ABS, ABS would have been the dispersed phase. For purposes of discussing the phase deformation during melt flow, an ABS domain that consisted of a composite rubber particle with some free SAN was considered. The crosslinked rubber particle was not highly deformable; only the free SAN with a viscosity lower than that of the continuous PC phase would have been highly deformed by the flow field. No matter how complex the flow field was, it could be separated into elongational and shear components. Under elongational flow, with axial extensional forces in the flow direction and compressive lateral forces, the free SAN was drawn out into strings while cohesive forces prevented the strings from breaking up. The molecular weight obtained for the free SAN component was in the range where theoretically a maximum in the extensibility of melt filaments was predicted[24]. It is also known that a deformable sphere will extend in a shear flow field, and the theoretical description of the phenomenon is well advanced[25]. The SAN/PC pair met the optimum conditions, in terms of viscosity ratio, that were described for extension of viscous drops into long threads[26].

The extension of SAN particles into long strings or threads was anticipated from the general understanding of particle motions in shear and elongational flow, and indeed the viscosities of the PC and free SAN were in the optimum range for formation of the long strings. The unique feature when ABS was the dispersed phase was the attachment of the SAN strings to the rubber particles as the free SAN was drawn out. Miscibility with the grafted SAN provided adhesion to the rubber particles. Continuous 'bead-and-string' structures of SAN 'strings' connecting rubber 'beads' could have formed if the original ABS domain contained more than one rubber particle or if several ABS domains coalesced during flow. Coalescence of a dispersed phase has been reported to occur under both elongational[27] and shear[28] flow conditions. This 'bead-and-string' morphology created the possibility for the ABS phase to be co-continuous with PC in the flow direction.

*Break-up of bead-and-string structure*

The proposed bead-and-string melt morphology of the ABS phase was sustained by the flow field; when the

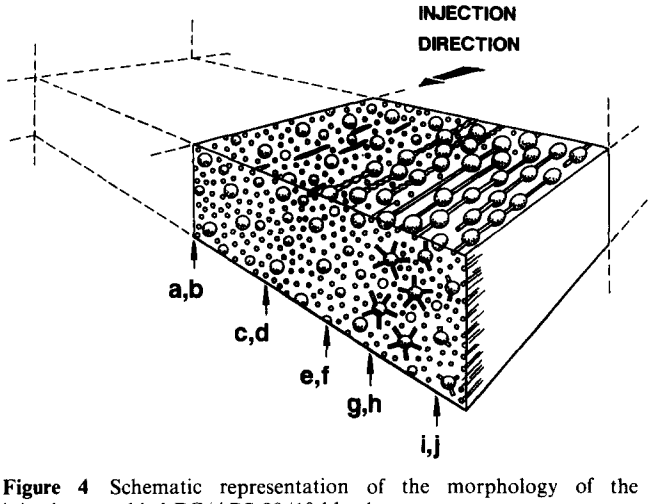


**Figure 4** Schematic representation of the morphology of the injection-moulded PC/ABS 90/10 blend

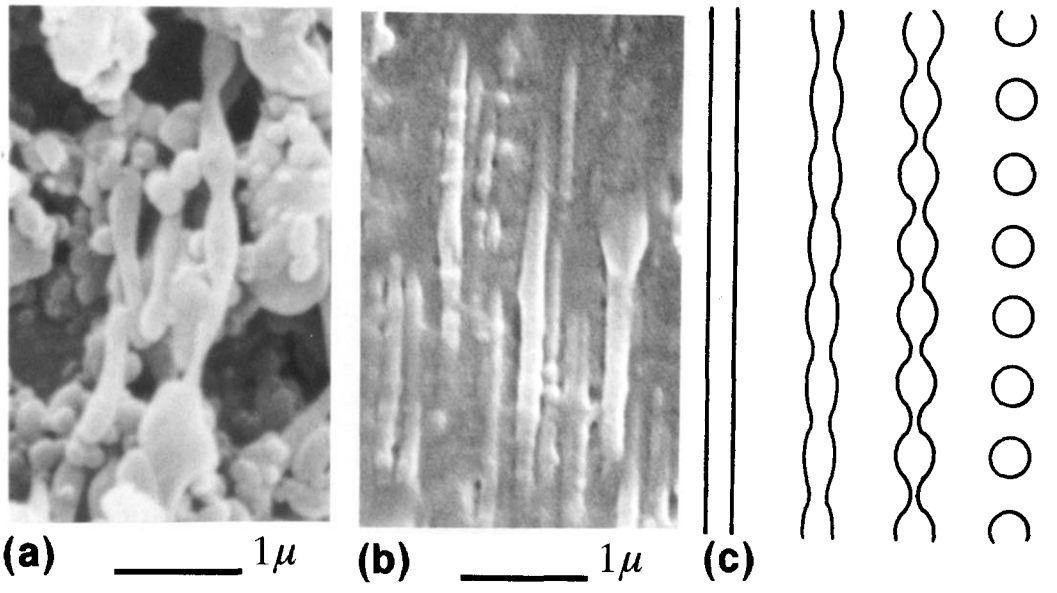


**Figure 5** Etched surfaces showing SAN strings in various stages of break-up: (a) parallel to the injection direction 1.05 mm from the edge; (b) parallel to the mould-contacting surface at a depth of 0.3 mm; and (c) schematic representation

flow conditions changed or flow ceased altogether, the bead-and-string morphology was affected. Although relaxation to a spherical shape was possible, viscous liquids such as SAN readjust their shape more slowly than less viscous fluids would, and instead can break up into many drops following the growth of Rayleigh instabilities[9–12]. It has been emphasized that this mechanism of interfacial-tension-driven break-up can occur after flow has ceased only when the aspect ratio of the thread is very large[29].

A striking feature reported in the break-up of stationary fluid threads was the simultaneous disintegration at all points along the thread into a series of drops[30]. Evidence that break-up of SAN strings followed the concepts developed in studies of lower-viscosity fluids appeared in an etched surface (*Figure 5*). The micrographs show shapes that are very similar to the intermediate stages of break-up envisaged in the literature[30]. *Figure 5a* shows a SAN string in an initial stage of break-up with undulations created by the instability, while *Figure 5b* contains several columns of uniform spheres about 0.3 μm in diameter that formed when the string disintegrated but had not had time to disperse.

End-pinching behaviour has been reported in fluid threads with bulbous ends[31]. In this special case, the bulbous end broke off from the central portion of the thread due to capillary forces associated with curvature variations along the interface, rather than by a capillary wave instability[31,32]. Because of the curvature at the conjunction of the SAN string with the rubber particle, this mechanism could have caused separation of the SAN string from the rubber particle during relaxation in a separate process from break-up of the SAN string.

The range of flow conditions and cooling rates through the thickness of the plaque during the injection moulding operation made it possible to find evidence for the various stages of end pinching and break-up in the micrographs. An example of the beginning of end pinching with constriction at the point of union of a rubber particle and SAN string was seen in *Figure 6a*; in another example, the pointed end of the SAN string in *Figure 6b* suggested that it had just broken off from the nearby rubber particle; and in *Figure 6c* the appearance of the SAN strings suggested that they were at a stage after detachment when the pointed ends had relaxed to a bulbous shape and instability that would lead to break-up of the SAN string was beginning.

*Effect of annealing*

Some evidence for break-up of the bead-and-string structure after cessation of flow was obtained when the micrographs revealed instances of intermediate stages of break-up frozen into the injection-moulded plaque. The hypothesis that the bead-and-string structure was sustained by the flow field and was only retained after moulding because rapid cooling did not permit sufficient time for relaxation was tested by observing the effect of annealing on the morphology. *Figure 7* shows the changes near the edge, where the bead-and-string structure was retained in the injection-moulded plaque, after annealing for a short period of time, nominally 12 s. The initial bead-and-string structure (*Figure 7a*) was only slightly altered after heating to 185°C by the appearance of a few small spherical SAN particles (*Figure 7b*); but after heating only 15°C higher, to 200°C, the bead-and-string structure had disappeared (*Figure 7c*) and instead of the long thin SAN strings there were numerous small spherical SAN particles while only remnants of thicker SAN strings remained. These were mostly separated from the rubber particles and often had bulbous ends and undulations in cross-section as if they were in the process of breaking up. A temperature of 270°C for nominally 12 s was sufficient for the bead-and-string structure to break up completely into small spherical SAN particles (*Figure 7d*); in this instance only the linear arrangement of the SAN particles remained to show that they had originated from elongated strings.

The morphology of the annealed specimens was examined at other locations through the thickness. The regions where the morphology was examined were as close as possible to the heating element of the d.s.c. so

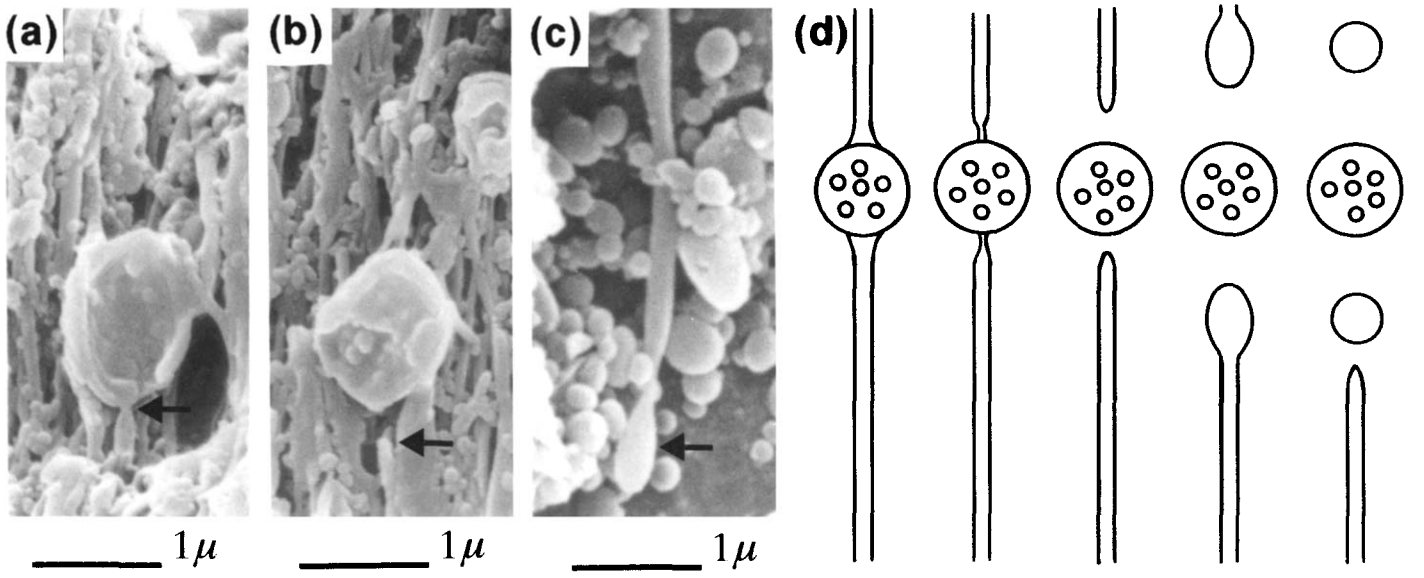


**Figure 6** Etched surfaces showing various stages of end pinching: (a) constriction at the junction of the rubber bead and SAN string; (b) the SAN string separated from the rubber bead; (c) relaxation of the end of a separated SAN string into a bulbous shape; and (d) schematic representation

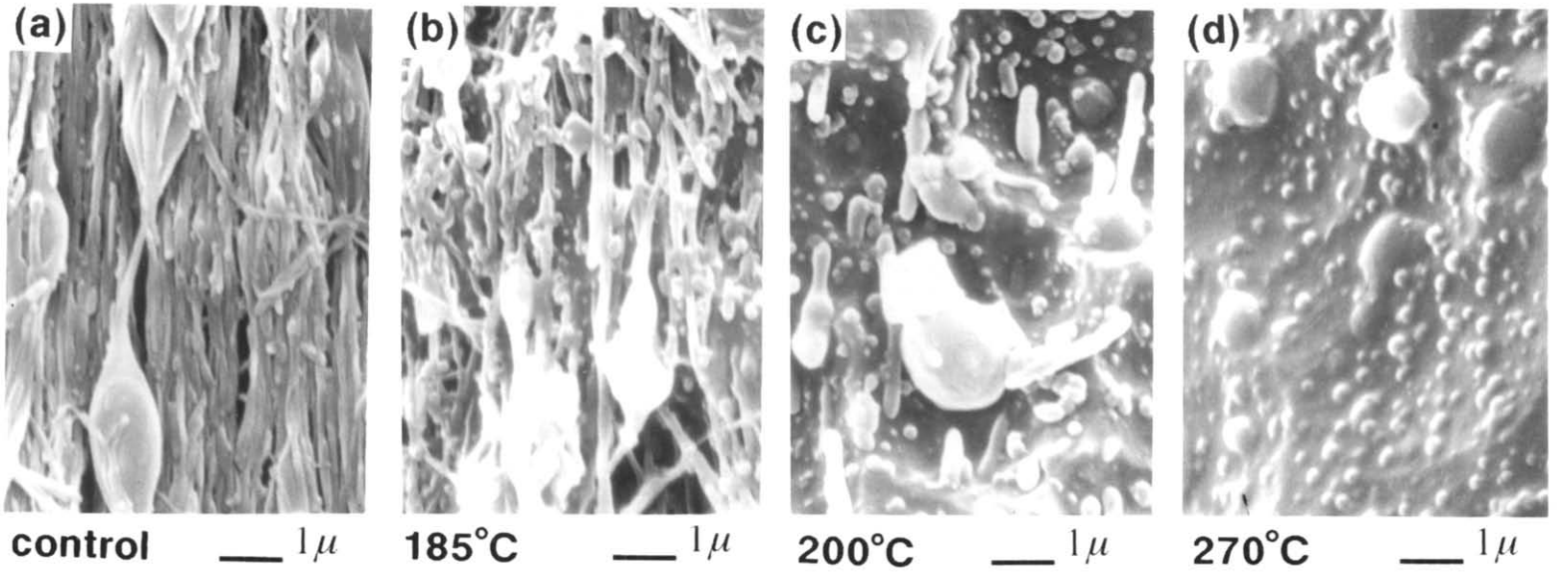


**Figure 7** The annealed blend viewed parallel to the injection direction near the edge of the plaque; specimens were annealed for nominally 12 s and etched with aqueous KOH: (a) the unannealed control, (b) annealed at 185°C, (c) at 200°C and (d) at 270°C

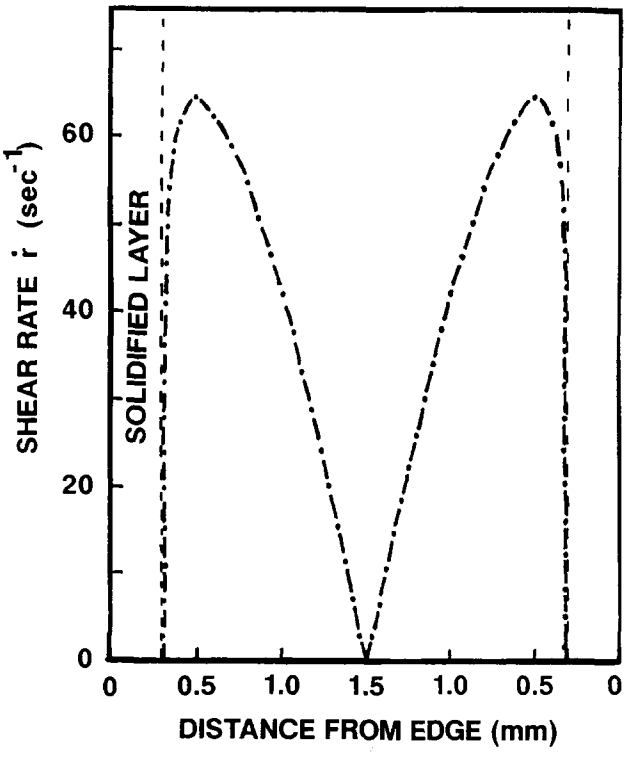


**Figure 8** Shear rate profile through the thickness during mould filling, estimated for the PC/ABS 90/10 blend[1]

that the thermal history was as similar as possible for all locations. The morphology gradient through the thickness was completely removed by annealing at 270°C for nominally 6 s, the shortest holding time available on the d.s.c.; under these conditions, the bead-and-string structure broke up completely and spherical SAN particles were observed through the entire thickness.

The bead-and-string structure broke up more slowly away from the edge. For example, 0.45 mm inward from the edge of the specimens annealed at 185 and 200°C for 12 s, the appearance of a few spherical SAN particles was evidence for the beginning of break-up, but the bead-and-string structure did not break up completely until the highest annealing temperature. The longer break-up time was attributed to the larger diameter of SAN strings at this location.

*Origin of the morphology gradient*

The melt morphology of the ABS phase as the blend entered the mould was determined to be the bead-and-string structure. This conclusion was based on SEM observations of etched material from the tab, which was assumed to have cooled rapidly enough to preserve the melt flow morphology in the gate. It was reasonable that dispersed ABS domains, formed in previous blending operations, would have elongated and coalesced into the bead-and-string structure in the high shear and elongational flow fields the melt experienced prior to entering the mould. The subsequent evolution to the final solid-state structure was determined by the flow fields experienced by the melt during mould filling, and the cooling rate during and after mould filling. Since injection moulding is not a steady-state operation, these were not known precisely and only a qualitative analysis was attempted.

In the case of non-isothermal flow, the velocity distribution through the thickness has an inflection point where the shear rate attains a maximum[1,33,34], while the shear rate is zero at the mould surface and at the centre. The shear-rate profile some distance behind the advancing front (*Figure 8*) was estimated from the approximate method described in the literature[1]. In the region of higher shear rates, which occupied the largest portion of the thickness, the bead-and-string structure was probably retained during mould filling. Only near the centre in the low-shear-rate region was the bead-and-string structure expected to break up by the instability and end-pinching mechanisms during mould filling.

The centre region was only a small part of the thickness, but because the velocity was highest, this region provided material to the advancing melt front where the fountain flow pattern developed[1]. In the fountain pattern, elongational flow perpendicular to the injection direction carries material from the centre to the mould surface, where it solidifies rapidly to form the characteristic skin layer[1]. It was thought likely that even though the ABS phase probably broke up into a dispersed particulate morphology in the centre during mould filling, the bead-and-string structure would re-form under the elongational flow field at the melt front and subsequently be preserved in the skin layer that solidified upon contact with the cold mould surface. The schematic representation in *Figure 9* illustrates the proposed formation of the bead-and-string structure at the melt front.

Indirect evidence to support this supposition was obtained by examining the morphology at the un-gated end of the mould where the melt front impinged and solidified rapidly when the mould was completely filled. In the centre of the thickness at this location, the morphology of the free SAN phase consisted primarily of a dispersion of small particles, the expected product of bead-and-string break-up, together with a few SAN strings attached to rubber particles. Between the centre and the edge, bead-and-string structures that could have formed by coalescence and extension of the spherical particles were obtained, but these were oriented normal to the mould-contacting surface along the flow lines at the front of the fountain flow.

Since the bead-and-string structure extended through the thickness approximately half the distance to the

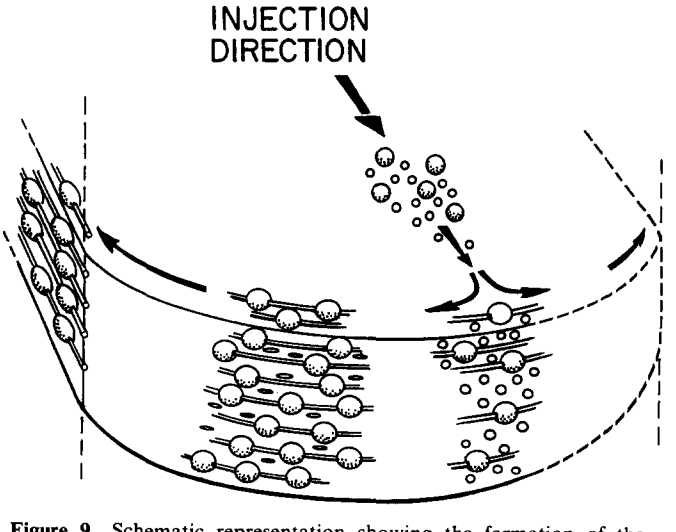


**Figure 9** Schematic representation showing the formation of the bead-and-string structure at the melt front

centre, it was thought to be derived from both the elongational flow at the melt front and the shear flow behind the melt front. The region closest to the edge that derived from the elongational flow at the melt front was discernible by the subtle change in the bead-and-string structure about 0.2 mm from the edge. The calculated thickness of the skin layer that had solidified at the end of mould filling was in the range of 0.24 to 0.34 mm[35–38], in good agreement with the observed dimension.

In the region between the skin layer that derived from the melt front, where solidification was rapid and the melt morphology was largely retained, and the centre, where the low shear rate during mould filling and long cooling time after mould filling assured relaxation to the particulate morphology, the final solid-state morphology was determined by the competition between the break-up rate and the cooling rate. A method in the literature was used to estimate the temperature gradient through the thickness of the melt at the conclusion of the mould filling stage and at various times thereafter during cooling[38]. The melt diffusivity of PC was taken from the literature[39]. In the calculations it was assumed that at the end of mould filling the temperature varied from approximately the $T_g$ of PC, 150°C, at the skin layer to the temperature of the melt when it entered the mould, 270°C, at the centre. In this way, it was estimated that the temperature in the centre of the mould reached the $T_g$ of PC in about 12–13 s.

It was known from the isothermal annealing experiments that even if the temperature exceeded the $T_g$ of PC at the end of mould filling, break-up might not have occurred during mould cooling. In particular, in the region where the temperature at the end of mould filling was of the order of 185–200°C, the bead-and-string structure would not have broken up even if the temperature had remained constant for the approximately 12 s cooling time. Since the temperature in the mould in fact was continuously decreasing, it was even less likely that the bead-and-string structure would have had time to break up in this region. From the calculations, it was estimated that the 185–200°C temperature range was achieved at the end of mould filling about 0.5 mm inward from the edge. Examination of the morphology showed no evidence of break-up at this position.

Evidence of break-up, specifically the appearance of some spherical SAN particles, was only observed when the depth was greater than 0.5 mm from the edge. The amount of break-up was expected to vary from relatively little at the 0.5 mm position, where the melt temperature was initially lower and less time was required to cool to 150°C, to almost complete break-up near the centre, where the temperature was initially highest and the cooling time longest. Thus a gradient was created through the thickness with various amounts of break-up by the instability and end-pinching mechanisms as seen in the micrographs (cf. *Figure 1*). This gradient was also observed by the gradual increase in the number of SAN spheres from almost zero at 0.5 mm to the very large number observed at the centre of the plaque (cf. *Figure 3*).

## CONCLUSIONS

The phase morphology of a PC/ABS 90/10 blend in injection-moulded plaques was characterized. Examination of etched brittle fracture surfaces led to a description and explanation of the morphology gradient through the thickness: in the centre of the plaque, the morphology was isotropic with the ABS phase dispersed in the PC matrix as large composite rubber particles and smaller spherical SAN particles. About half the distance from the centre to the edge, the morphology of the free SAN changed from predominantly spherical to predominantly string-like. The SAN strings connected the rubber particles to form an oriented ABS bead-and-string structure that was essentially continuous in the injection direction.

The melt morphology of the ABS phase as the blend entered the mould was determined to be the bead-and-string structure. It was thought that this morphology was sustained during mould filling in regions of high elongational and high shear flow.

The gradient in phase morphology was created by the competition between the relaxation rate of the bead-and-string structure and the cooling rate after mould filling. It was proposed that the bead-and-string structure was retained in the region where the melt experienced the highest elongational and shear flows during mould filling, and solidified most rapidly during cooling.

Near the centre, where the shear rate was lowest and cooling time longest, it was proposed that the bead-and-string structure broke up by interfacial-tension-driven break-up and end-pinching mechanisms to produce the isotropic dispersion of 1 $\mu$m composite rubber particles and 0.3 $\mu$m free SAN particles.

## ACKNOWLEDGEMENT

This research was generously supported by The Dow Chemical Company.

## REFERENCES

1 Tadmor, Z. *J. Appl. Polym. Sci.* 1974, **18**, 1753
2 Karger-Kocsis, J. and Csikai, I. *Polym. Eng. Sci.* 1987, **27**, 241
3 Skochdopole, R. E., Finch, C. R. and Marshall, J. *Polym. Eng. Sci.* 1987, **27**, 627
4 McLaughlin, K. W. *Polym. Eng. Sci.* 1989, **29**, 1560
5 Tsebrenko, M. V., Rezanova, N. M. and Vinogradov, G. V. *Polym. Eng. Sci.* 1980, **20**, 1023
6 Quintens, D., Groeninckx, G., Guest, M. and Aerts, L. *Polym. Eng. Sci.* 1991, **31**, 1207, 1215
7 Karger-Kocsis, J., Kallo, A. and Kuleznev, V. N. *Polymer* 1984, **25**, 279
8 Elmendorp, J. J. *Polym. Eng. Sci.* 1986, **26**, 418
9 Rayleigh, J W. S. *Proc. R. Soc.* 1879, **29**, 71
10 Taylor, G. I. *Proc. R. Soc. Lond.* (*A*) 1934, **146**, 501
11 Tomotika, S. *Proc. R. Soc. Lond.* (*A*) 1935, **150**, 322
12 Tomotika, S. *Proc. R. Soc. Lond.* (*A*) 1936, **153**, 308
13 Kurauchi, T. and Ohta, T. *J. Mater. Sci.* 1984, **19**, 1699
14 Suarez, H., Barlow, J. W. and Paul, D. R. *J. Appl. Polym. Sci.* 1984, **29**, 3253
15 Kim, W. N. and Burns, C. M. *Polym. Eng. Sci.* 1988, **28**, 1115
16 Moore, L. D., Moyer, W. W. and Frazer, W. J. *J. Appl. Polym. Sci., Appl. Polym. Symp.* 1968, **7**, 67
17 Post, M. A. *J. Paint Tech.* 1966, **38**, 336
18 Wexler, A. S. *Anal. Chem.* 1964, **36**, 1829
19 Weir, A. P., Williams, D. A. and Woodstock, J. D. *Chem. Ind.* 1971, **35**, 990
20 Casale, A., Moroni, A. and Spreafico, C. *ACS Polym. Prepr.* 1974, **15**(1), 334
21 Mendelson, R. A. *Polym. Eng. Sci.* 1976, **16**, 690
22 Shenoy, A. V. and Saini, D. R. *Rheol. Acta* 1984, **23**, 368
23 Saini, D. R. and Shenoy, A. V. *J. Macromol. Sci.–Phys.* (*B*) 1983, **22**, 437
24 Ide, Y. and White, J. L. *J. Appl. Polym. Sci.* 1976, **20**, 2511

25 Torza, S., Cox, R. G. and Mason, S. G. *J. Colloid Interface Sci.* 1972, **38**, 395
26 Rumscheidt, F. D. and Mason, S. G. *J. Colloid Sci.* 1961, **16**, 238
27 Tsebrenko, M. V., Yudin, A. V., Ablazova, T. I. and Vinogradov, G. V. *Polymer* 1976, **17**, 831
28 Elmendorp, J. J. and Van der Vegt, A. K. *Polym. Eng. Sci.* 1986, **26**, 1332
29 Stone, H. A. and Leal, L. G. *J. Fluid Mech.* 1989, **198**, 399
30 Rumscheidt, F. D. and Mason, S. G. *J. Colloid. Sci.* 1962, **17**, 260
31 Stone, H. A. and Leal, L. G. *J. Fluid Mech.* 1989, **206**, 223
32 Goedde, E. F. and Yuen, M. C. *J. Fluid Mech.* 1970, **40**, 495
33 Kamal, M. R. and Kenig, S. *Polym. Eng. Sci.* 1972, **12**, 302
34 White, J. L. *Polym. Eng. Sci.* 1975, **15**, 44
35 Barrie, I. T. *Plast. Polym.* 1968, **37**, 463
36 Churchill, S. W. and Evans, L. B. *J. Heat Transfer* 1971, **93**, 234
37 White, J. L. and Dietz, W. *Polym. Eng. Sci.* 1979, **19**, 1081
38 Carslaw, H. S. and Jaeger, J. C. 'Conduction of Heat in Solids', 2nd Edn., Oxford University Press, New York, 1973
39 Tadmor, Z. and Gogos, C. G. 'Principles of Polymer Processing', Wiley-Interscience, New York, 1979, Ch. 5, p. 132